JOURNAL OF GEOPHYSICAL RESEARCH, VOL. 114, A00C17, doi:10.1029/2008JA013505, 2009

Magnetic island formation between large-scale flow vortices at an undulating postnoon magnetopause for northward interplanetary magnetic field

S. Eriksson,[1] H. Hasegawa,[2] W.-L. Teh,[3] B. U. Ö. Sonnerup,[3] J. P. McFadden,[4] K.-H. Glassmeier,[5] O. Le Contel,[6] V. Angelopoulos,[4] C. M. Cully,[7] D. E. Larson,[4] R. E. Ergun,[1] A. Roux,[6] and C. W. Carlson[4]

Received 15 June 2008; revised 12 November 2008; accepted 25 November 2008; published 21 February 2009.

[1] Time History of Events and Macroscale Interactions during Substorms multispacecraft observations are presented for a ~2-h-long postnoon magnetopause event on 8 June 2007 that for the first time indicate that the trailing (sunward) edges of Kelvin-Helmholtz (KH) waves are commonly related to small-scale <0.56 R_E magnetic islands or flux transfer events (FTE) during the growth phase of these surface waves. The FTEs typically show a characteristic bipolar B_N structure with enhanced total pressure at their center. Most of the small-scale FTEs are not related to any major plasma acceleration. TH-A observations of one small FTE at a transition from the low-latitude boundary layer (LLBL) into a magnetosheath plasma depletion layer were reconstructed using separate techniques that together confirm the presence of a magnetic island within the LLBL adjacent to the magnetopause. The island was associated with a small plasma vortex and both features appeared between two large-scale (~1 R_E long and 2000 km wide) plasma vortices. We propose that the observed magnetic islands may have been generated from a time-varying reconnection process in a low ion plasma beta ($\beta_i < 0.2$) and low 8.3° field shear environment at the sunward edge of the growing KH waves where the local magnetopause current sheet may be compressed by the converging flow of the large-scale plasma vortices as suggested by numerical simulations of the KH instability.

Citation: Eriksson, S., et al. (2009), Magnetic island formation between large-scale flow vortices at an undulating postnoon magnetopause for northward interplanetary magnetic field, *J. Geophys. Res.*, *114*, A00C17, doi:10.1029/2008JA013505.

1. Introduction

[2] The Kelvin-Helmholtz instability (KHI) is expected to grow along the flank magnetopause because of the local shear between the tailward magnetosheath flow and the stagnant or sunward flow in the equatorial outer magnetosphere. It has been studied extensively for understanding various magnetospheric phenomena, such as momentum or mass transport from the solar wind into the magnetosphere [e.g., *Miura*, 1984; *Fujimoto and Terasawa*, 1994].

[3] Observational evidence of magnetopause surface waves excited by the KHI that propagate antisunward has been reported for some time [e.g., *Sckopke et al.*, 1981; *Fairfield et al.*, 2000, and references therein]. Recent multispacecraft observations by Cluster [*Hasegawa et al.*, 2004] have demonstrated that the KHI grows nonlinearly along the flank magnetopause to form large-scale rolled up plasma vortices for prolonged northward interplanetary magnetic field (IMF) conditions. Such vortices are believed to be a key ingredient for efficient solar wind plasma entry into the magnetosphere during northward IMF [e.g., *Fairfield et al.*, 2000]. Large-amplitude KH vortices are now known to be a rather common feature along the flank magnetopause beyond the dawn-dusk terminator for northward IMF [*Hasegawa et al.*, 2006a].

[4] Numerical simulations predict that non-MHD processes, e.g., magnetic reconnection, may become effective in the vicinity of KH vortices and can lead to transport or mixing of plasmas [e.g., *Pu et al.*, 1990; *Otto and Fairfield*, 2000; *Brackbill and Knoll*, 2001; *Nykyri and Otto*, 2001; *Knoll and Brackbill*, 2002; *Nykyri and Otto*, 2004; *Nakamura et al.*, 2006, 2008]. However, very little is known about these microphysical processes in and around the KH vortices from an observational point of view. *Nykyri et al.* [2006] found in situ evidence of reconnection within KH vortices

[1]Laboratory for Atmospheric and Space Physics, University of Colorado, Boulder, Colorado, USA.
[2]Department of Space Plasma Physics, Institute of Space and Astronautical Science, Japan Aerospace Exploration Agency, Sagamihara, Japan.
[3]Thayer School of Engineering, Dartmouth College, Hanover, New Hampshire, USA.
[4]Space Sciences Laboratory, University of California, Berkeley, California, USA.
[5]Institut für Geophysik und Extraterrestrische Physik, Technische Universität, Braunschweig, Germany.
[6]Laboratoire de Physique des Plasmas, École Polytechnique, Palaiseau, France.
[7]Swedish Institute of Space Physics, Uppsala, Sweden.

0148-0227/09/2008JA013505$09.00

in the form of satisfied Walén relations [e.g., *Sonnerup et al.*, 1987] and ion beams in the velocity distributions. This study, however, could not establish a clear causal connection between the KHI and the identified reconnection signatures. Important questions thus remain as to how reconnection initiates in connection with surface waves and at what stage of the KHI development.

[5] This report provides new evidence from the Time History of Events and Macroscale Interactions during Substorms (THEMIS) mission [*Angelopoulos*, 2008] suggesting that small-scale flux transfer events (FTE) [e.g., *Russell and Elphic*, 1979; *Sonnerup*, 1987] may be generated predominantly at the sunward edge of KH waves (rather than at the tailward edge) during their growth phase in the equatorial postnoon magnetopause region. FTEs are often assumed to be a signature of a time-dependent reconnection rate [e.g., *Paschmann et al.*, 1982; *Sonnerup*, 1987; *Scholer*, 1988; *Phan et al.*, 2005] and we adopt this assumption in our interpretations of the postnoon THEMIS observations on 8 June 2007.

2. Overview of THEMIS Observations and Solar Wind Conditions

[6] The five spacecraft of the THEMIS mission were launched into a near-equatorial orbit on 17 February 2007. These probes are referred to as TH-A, TH-B, TH-C, TH-D and TH-E. The initial coast phase of the mission with all five probes in the same 1.1 by 15.4 R_E string-of-pearls configuration lasted until mid-September 2007, with TH-B leading and TH-A trailing. The individual orbits were then changed over time to a configuration optimized for the magnetotail substorm physics goal of the mission. Figure 1 shows the postnoon positions of the five inbound THEMIS probes during the 0600–0900 UT period on 8 June 2007 as represented by their different colors. The first magnetopause transition of each individual probe is indicated by a diamond symbol.

[7] Figures 2a–2e display the time-shifted IMF (ACE) and solar wind conditions (ACE and Wind) during the 9.5-h-long 0330–1300 UT period on 8 June 2007. Figures 2f and 2g show the magnetic field measured by the TH-A Fluxgate Magnetometer (FGM) instrument [*Auster et al.*, 2008], while Figure 2h shows the TH-A ion energy-time spectrogram recorded by the ion Electro Static Analyzer (ESA) instrument [*McFadden et al.*, 2008a]. The ACE data were shifted forward in time by 66.5 min to optimize the match between the ACE IMF clock angle, $\theta = arctan(B_y/B_z)$, and the corresponding clock angle recorded by the TH-A FGM instrument in the solar wind and magnetosheath until ~0630 UT (see Figures 2f and 2h). The Wind data were time shifted by ~87 min to match the ACE solar wind plasma data.

[8] The vertical dotted line at 0645 UT marks the beginning of a ~2-h-long period of significant fluctuations at the TH-A location between a magnetosheath-like region and a region of high-energy magnetospheric ions coincident with ions of magnetosheath origin which is characteristic of the dayside low-latitude boundary layer (LLBL). TH-A eventually entered the plasma sheet (PS) after ~0930 UT. The ~0645 UT transition coincided with a sudden drop in solar wind density from N_P = 16.8 to 4.3 cm^{-3} and a corresponding drop in dynamic pressure, $P_{dyn} = \rho V^2$, from 3.4 to 0.9 nPa. The pressure drop is expected to result in an outward propagation of the magnetopause. The IMF magnitude also increased from 7.5 to 8.7 nT at this time (see Figure 2a) while the clock angle stayed nearly constant at $\theta_{IMF} = -19°$. The entire 0650–0900 UT period was characterized by a slow 355 km/s solar wind bulk speed and a strong northward IMF B_z = 7.7 nT with a fluctuating IMF $B_y < 0$ such that $-45° < \theta_{IMF} < 0°$.

[9] Figure 3 shows the TH-A ion energy-time spectrogram in the 0300–1000 UT interval, the corresponding magnitude of the magnetic field (B), and the power of magnetic field fluctuations in the 192 Hz frequency band from the THEMIS Search Coil Magnetometer (SCM) instrument [*Roux et al.*, 2008]. The 80–227 Hz passband of the 192 Hz filter has a maximum sensitivity at 144 Hz [*Cully et al.*, 2008]. Figures 3d and 3e show the ion plasma beta (β_i) and the Alfvén Mach number (M_A) when 3-s spin resolution fast survey mode ESA data [*McFadden et al.*, 2008a] are available. Figure 3 clearly indicates that any magnetosheath-like period encountered by TH-A during the 0645–0850 UT interval (between vertical dotted lines) was different in many aspects from the magnetosheath proper, which was characterized by $\beta_i > 1$, super-Alfvénic flow and significant power enhancements in the 192 Hz band. A majority of the enhancements display a clear correlation with local ~5 nT dips in the magnetic field magnitude (not shown) as expected for whistler-mode lion roars associated with mirror mode waves in the magnetosheath proper [e.g., *Tsurutani et al.*, 1982]. The power enhancements were typically nonexistent during the sub-Alfvénic magnetosheath-like intervals between 0645 and 0850 UT where $\beta_i < 0.2$ (lower β_i envelope). The weak power enhancements that did occur in the 192 Hz band mainly appeared at the steep B gradients across the magnetopause boundary.

[10] Figure 4 displays the 0615–0945 UT ion energy-time spectrograms from all THEMIS probes as well as the plasma density (N_P), magnetic field magnitude (B), plasma bulk speed (V) and the total plasma pressure ($P_{tot} = P_B + P_{Pi} + P_{Pe}$). The total speed is only available from TH-B and TH-A because of the higher fast survey telemetry mode [*Angelopoulos*, 2008] in which these probes operated until ~0915 UT.

[11] Several conclusions can be drawn from the multi-spacecraft observations in Figure 4. First, it is clear from the ion energy-time spectrograms that all probes (except perhaps TH-A) moved from the magnetosheath into the outer magnetosphere during a relatively short time period (TH-B at 0648:48 UT; TH-D at 0648:53 UT; TH-C at 0649:20 UT; TH-E at 0649:55 UT). This B-D-C-E sequence confirms an outward motion of the magnetopause (see Figure 1) in agreement with the dynamic pressure drop at this time (see Figure 2). Second, there was no clear evidence of a magnetosheath-like population at TH-B after the magnetopause crossing there, suggesting that TH-B ended up well inside the magnetosphere. This is confirmed by the low ($V <$ 50 km/s) plasma speed and the low ($N_P < 1$ cm^{-3}) plasma density after 0650 UT (see Figures 4f and 4h). TH-D observed magnetosheath-like plasmas coincident with higher-energy magnetospheric ions (LLBL) at ~0705 and ~0750 UT. The occurrence frequency of magnetosheath-like periods increased radially outward from TH-C to TH-A,

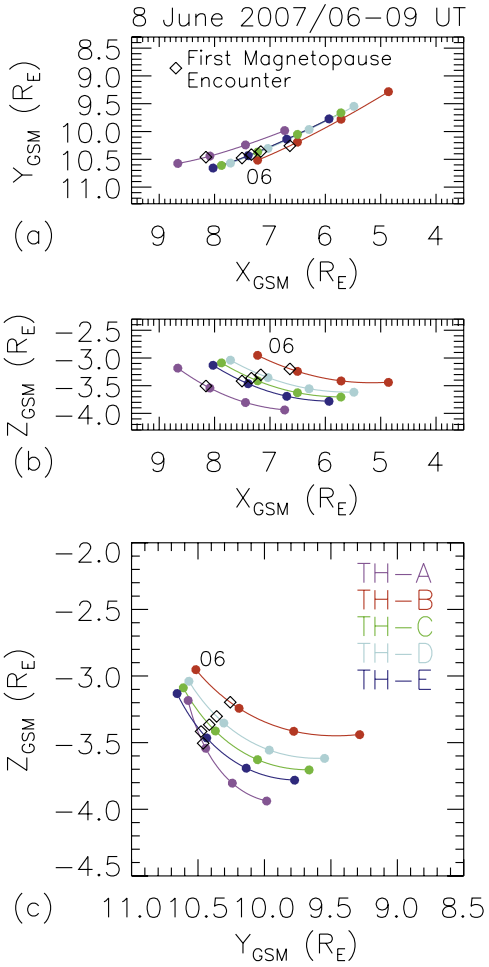

Figure 1. THEMIS multispacecraft positions are shown in GSM coordinates for the 0600–0900 UT period on 8 June 2007. Solid dots indicate probe positions at 0600, 0700, 0800, and 0900 UT. Diamond symbols mark the positions of the first magnetopause encounter for each probe.

which encountered numerous magnetopause transitions between the LLBL and the adjacent magnetosheath during 0650–0900 UT.

[12] The total plasma pressure was relatively constant below P_{tot} = 1 nPa after 0650 UT at all THEMIS probes, which indicates that the local magnetopause was at pressure balance during this time period. The fact that P_{tot} dropped from 1.19 to 0.69 nPa at ~0650 UT (TH-A) indicates that the magnetopause was not yet in pressure balance in agreement with an accelerated outward motion of the magnetopause following the sudden solar wind dynamic pressure drop at this time.

[13] The 0650–0850 UT magnetosheath-like TH-A observations indicate a lower N_P and a generally faster bulk speed V than observed by TH-A and TH-B in the magnetosheath before 0650 UT. Moreover, TH-A observed a maximum magnetic field strength in the B = 40–45 nT range during these magnetosheath-like intervals, that was similar to that measured by TH-B in the adjacent magnetosheath before 0650 UT. With the exception of the B observation (which should have been larger still) it may be argued that the N_P and V changes as seen by TH-A reflect the solar wind changes at this time (see Figure 2). However, this is not consistent with the larger differences seen after 0650 UT between the observed magnetic field clock angle (θ) at ACE and TH-A (see Figure 2f). The TH-A clock angle rather reflected an alignment between the geomagnetic and mag-

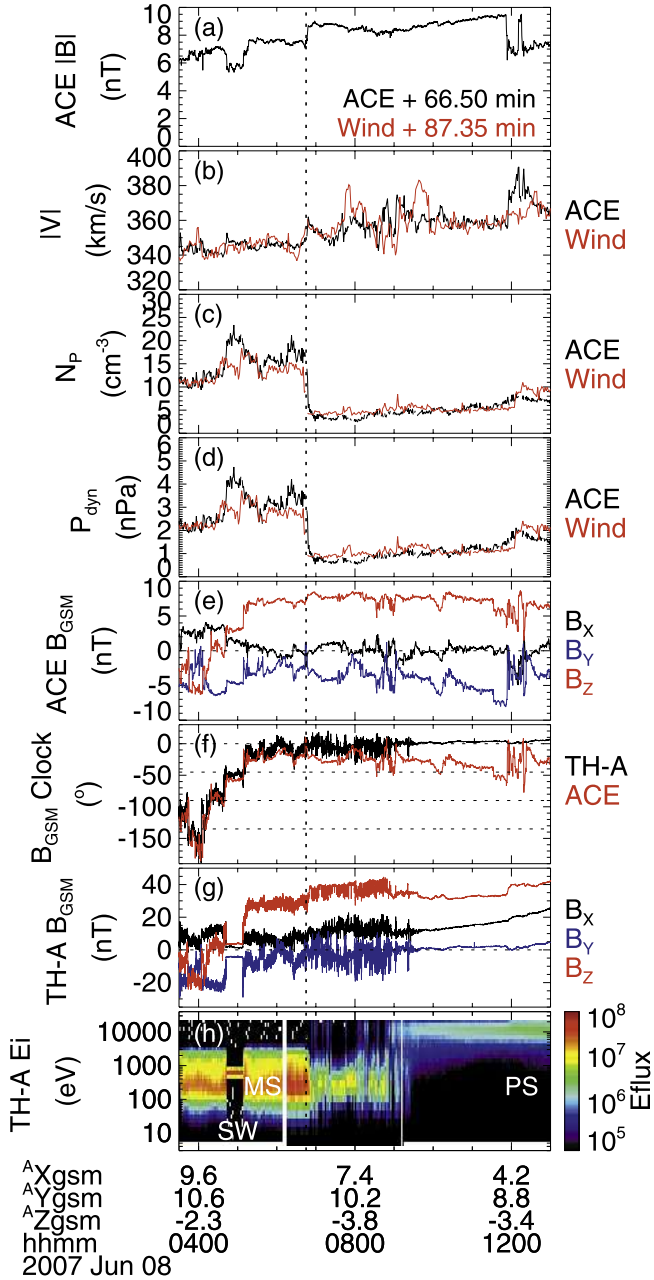

Figure 2. (a–d) ACE (black) and Wind (red) solar wind plasma and IMF data, (e) ACE IMF B_{GSM}, (f) ACE (red) and TH-A (black) GSM magnetic field clock angle (θ = $arctan(B_y/B_z)$), (g) TH-A GSM magnetic field, and (h) TH-A ion energy-time spectrogram with color showing the energy flux (Eflux) in eV/cm^2 s sr eV. The data are shown for the 0330–1330 UT period on 8 June 2007. The ACE (Wind) data were shifted by 66.50 (87.35) min to match the TH-A θ angle as recorded in the solar wind (SW) and magnetosheath (MS). Vertical dotted line marks the 0645 UT transition into a magnetopause boundary layer region.

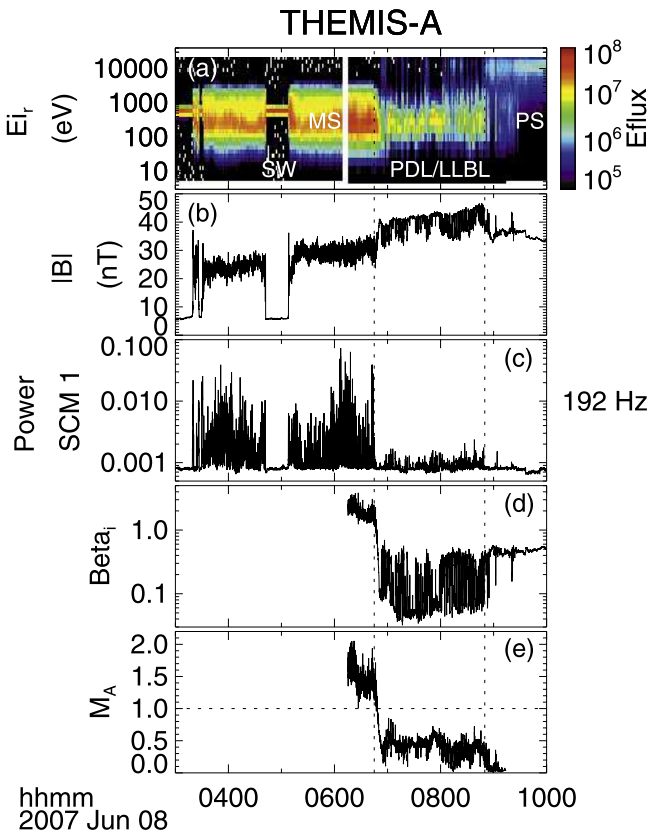

Figure 3. TH-A observations during the 0300–1000 UT period. (a) Ion energy-time spectrogram (energy flux in eV/cm^2 s sr eV), (b) magnetic field magnitude, (c) magnetic field fluctuations in the 192 Hz frequency passband (80–227 Hz range), (d) ion plasma beta (β_i), and (e) Alfvén Mach number. Vertical dotted lines are shown at 0645 and 0850 UT.

netosheath fields after 0650 UT. An alternative explanation is that TH-A entered a low-β_i and sub-Alfvénic (see Figure 3) magnetosheath plasma depletion layer (PDL) adjacent to the magnetopause [e.g., *Zwan and Wolf*, 1976; *Sibeck et al.*, 1990; *Wang et al.*, 2003; and references therein] which is expected to occur for strong northward IMF conditions such that the magnetosheath magnetic field is draped and compressed over the magnetopause.

[14] The PDL is expected to develop as the subsolar magnetopause reconnection rate decreases [*Anderson et al.*, 1997], resulting in a layer of compressed magnetic flux adjacent to the magnetopause. Plasma is removed from the PDL as a consequence of the enhanced magnetic pressure, and faster downtail magnetosheath speeds result from the release of magnetic field tension away from the subsolar stagnation region [e.g., *Sibeck et al.*, 1990; *Chen et al.*, 1993]. A high-latitude reconnection mechanism tailward of both cusps for northward IMF [*Dungey*, 1963; *Song and Russell*, 1992] may also remove some PDL plasma directly across the magnetopause by capturing it onto newly closed dayside flux.

[15] A PDL is consistent with the buildup of magnetic flux against the magnetopause for the prevailing northward IMF and the radial B profile that the THEMIS probes recorded in the 0615–0645 UT period (see Figure 4g) with an increasing magnetosheath B magnitude being observed with decreasing radial distance from TH-A (outermost probe) to TH-B (innermost probe). A PDL also explains the sub-Alfvénic flow regime as well as the suppression of magnetic field power in the 192 Hz frequency band after 0650 UT (see Figure 3). The lower β_i of the PDL likely

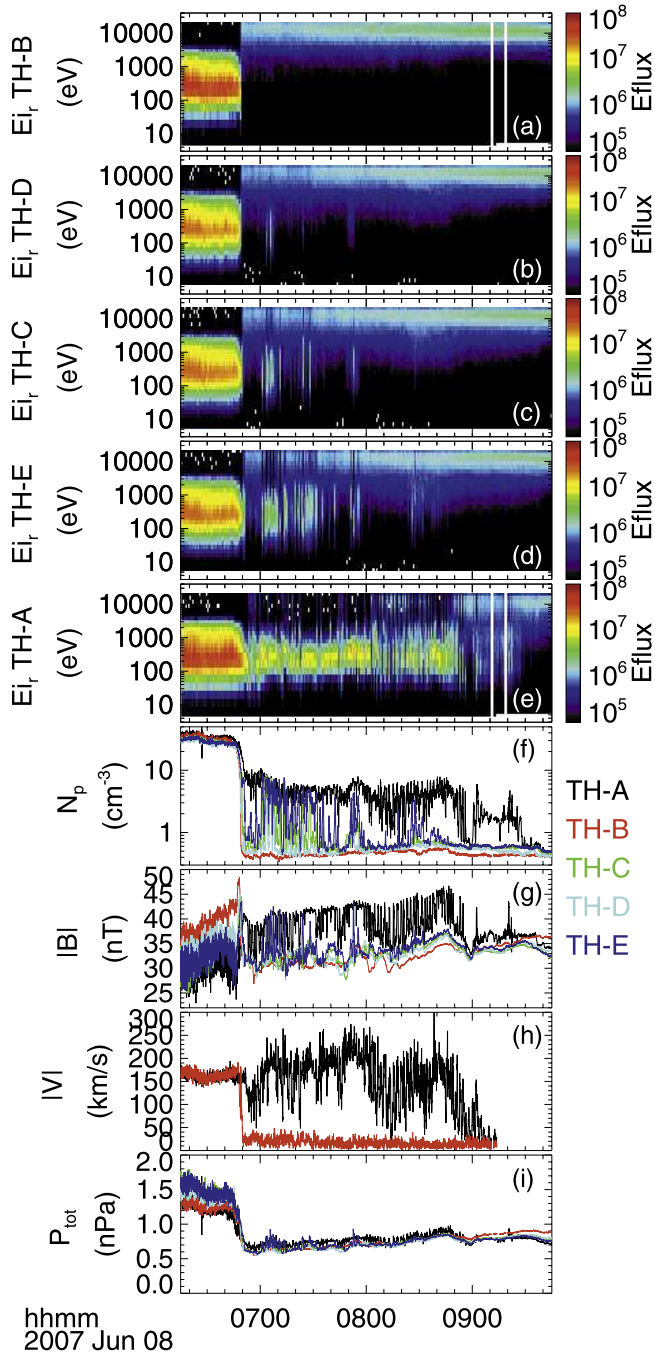

Figure 4. THEMIS observations from all five spacecraft are shown for the 0615–0945 UT period. (a–e) Ion energy-time spectrograms for TH-B, TH-D, TH-C, TH-E, and TH-A (energy flux shown in eV/cm^2 s sr eV); (f) ion plasma density assuming protons; (g) magnetic field magnitude; (h) plasma speed; and (i) total plasma pressure, $P_{tot} = P_B + P_{Pi} + P_{Pe}$.

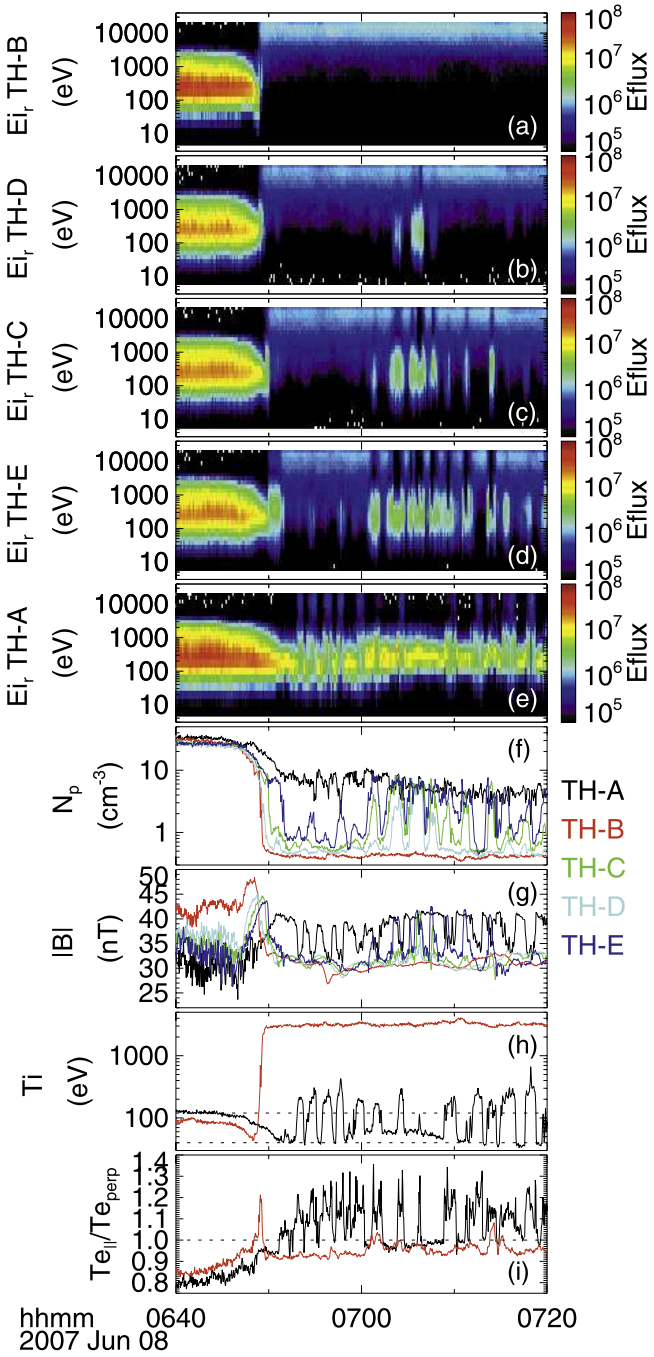

Figure 5. THEMIS observations from all five spacecraft are shown for the 0640–0720 UT period. (a–e) Ion energy-time spectrograms for TH-B, TH-D, TH-C, TH-E, and TH-A (energy flux in eV/cm^2 s sr eV); (f) ion plasma density assuming protons; (g) magnetic field magnitude; (h) average ion temperature where horizontal dotted lines mark Ti = 40 and 120 eV; and (i) electron temperature anisotropy ratio.

quenched the mirror mode turbulence of the upstream magnetosheath [*Anderson and Fuselier*, 1993] and the associated whistler mode emissions in the 192 Hz band [*Tsurutani et al.*, 1982]. On the other hand, it is unclear how the observed solar wind changes alone would result in $\beta_i <$ 0.2, sub-Alfvénic flow and the suppression of 192 Hz lion roars and mirror mode fluctuations.

[16] Figure 5 provides a shorter (40-min) interval of the THEMIS data shown in Figure 4 near the 0650 UT magnetopause transition with the exception of the speed and total pressure data, which have been replaced by the average ion temperature (Ti) and the electron temperature anisotropy ratio ($Te_{\|}/Te_{\perp}$) at TH-B and TH-A. Figure 5 highlights the presence of surface waves in the ion energy-time spectrograms at the magnetopause boundary and also at the inner boundary of the LLBL. It is clear that only TH-A observed magnetopause waves during the 0653–0658 UT period (interval I), while at the same time TH-E observed transitions between the LLBL and the plasma sheet. An approximate LLBL thickness can therefore be estimated for interval I as the separation between TH-A and TH-E along the magnetopause normal direction.

[17] During 0703–0708 UT (interval II), TH-A was farther away from the magnetopause and immersed deeper into the PDL and only observed one LLBL encounter. Meanwhile, the intermediate TH-E and TH-C probes observed frequent magnetopause surface wave activity. TH-D did not encounter the magnetopause and rather transitioned between the LLBL and the plasma sheet. Interval II may therefore be used to estimate the amplitude of the magnetopause surface waves.

[18] Probe separations along the normal direction relative to TH-A (first period) and TH-E (second period) are listed in Table 1. Interval I indicates a normal LLBL thickness of about 0.52 R_E or 3308 km from the separation between TH-A and TH-E. Although the respective outer and inner LLBL transitions at TH-A and TH-E occurred almost simultaneously, it is emphasized that the two probes were also separated by 0.46 R_E (2900 km) along the magnetopause. The waves at the outer and inner edge of the LLBL were thus out of phase in a spatial sense. Interval II suggests that the amplitude of the magnetopause surface waves (D_{MP}) was in the range 0.18 < D_{MP} < 0.91 R_E or 1157 < D_{MP} < 5776 km, since TH-E and TH-C observed the waves, but neither TH-A (in the magnetosheath), nor TH-D (in the LLBL) did so.

[19] The Ti and $Te_{\|}/Te_{\perp}$ profiles measured by TH-B and TH-A in the magnetosheath before ~0650 UT are nearly identical. TH-A was located farther out in a relatively warmer magnetosheath proper than TH-B at this time, where Ti = 120 eV (upper horizontal dotted line in Figure 5h) and $Te_{\|} < Te_{\perp}$, which is often observed in the magnetosheath [*Phan et al.*, 1996]. The observed time delay between the two magnetosheath profiles (TH-B leading TH-A) for both Ti and $Te_{\|}/Te_{\perp}$ is consistent with their relative distances from the magnetopause and the fact that TH-B reached the magnetopause region before TH-A because of the outward boundary propagation.

[20] A cold Ti = 40 eV (lower dotted line in Figure 5h) ion population was measured in the adjacent magnetosheath just before TH-B crossed the magnetopause into the hot Ti > 3000 eV plasma sheet. TH-A clearly did not reach that far into the magnetosphere following the magnetopause expansion and rather spent a considerable amount of time in the same cold Ti ~ 40 eV magnetosheath-like region that TH-B encountered where the electrons were characteristically more isotropic ($Te_{\|} \sim Te_{\perp}$) than in the outer magnetosheath. Cold ions are consistent with a PDL due to the gradual evacuation of the magnetosheath plasma. It is the cold Ti of

Table 1. Relative Average Probe Separations Along Average Boundary Normal Directions for Two Magnetopause Surface Wave Intervals on 8 June 2007[a]

THEMIS	ΔR_N[b] (R_E)	ΔR_N (km)	ΔR_M (R_E)	ΔR_M (km)	ΔR_L (R_E)	ΔR_L (km)
Interval I 0653–0658 UT Using TH-A LMN Directions[c]						
TH-B	1.365	8704	0.865	5516	0.003	20
TH-D	0.883	5632	0.596	3800	0.007	44
TH-C	0.696	4437	0.520	3319	0.025	160
TH-E	0.519	3308	0.455	2901	0.039	247
Interval II 0703–0708 UT Using TH-E LMN Directions[d]						
TH-B	0.866	5525	0.415	2645	−0.038	−243
TH-D	0.374	2383	0.144	920	−0.033	−210
TH-C	0.181	1157	0.067	429	−0.014	−90
TH-A	−0.532	−3393	−0.454	−2898	−0.037	−239

[a]Distances are positive toward TH-A (interval I) and TH-E (interval II) along their respective TH-A and TH-E LMN directions.
[b]One Earth radius is defined as R_E = 6378.16 km.
[c]TH-A: $\hat{\mathbf{N}}^A_{GSM}$ = (0.7307, 0.6471, −0.2177), $\hat{\mathbf{M}}^A_{GSM}$ = (0.6630, −0.7486, 0.0000), and $\hat{\mathbf{L}}^A_{GSM}$ = (0.1630, 0.1443, 0.9760).
[d]TH-E: $\hat{\mathbf{N}}^E_{GSM}$ = (0.7240, 0.6540, −0.2193), $\hat{\mathbf{M}}^E_{GSM}$ = (0.6704, −0.7420, 0.0000), and $\hat{\mathbf{L}}^E_{GSM}$ = (0.1627, 0.1470, 0.9757).

the PDL that balances the locally higher magnetic field pressure there, consistent with the local field magnitude enhancements that all probes observed just outside the magnetopause. It is likely that the PDL region is responsible also for the isotropization of the magnetosheath electrons which in turn quench the free energy source of the whistler mode wave growth that require $Te_{\|} < Te_{\perp}$.

[21] Each LLBL interval encountered by TH-A is related to warmer $Ti > 200$ eV ions and $Te_{\|} > Te_{\perp}$ electrons which are often observed in the LLBL [e.g., *Paschmann et al.*, 1993]. $Te_{\|} > Te_{\perp}$ indicates that these flux tubes may have been connected to a high-latitude reconnection region for northward IMF that heats the cold incoming magnetosheath electrons in the field-aligned direction [e.g., *Lavraud et al.*, 2005; *McFadden et al.*, 2008b].

[22] The four leading THEMIS probes encountered a temporary field enhancement in close proximity to each individual magnetopause transition while TH-A lingered in this high-B region. We interpret the regions of enhanced B as PDL field compressions ahead of the radially expanding magnetopause surface rather than an increased IMF magnitude (see Figure 2). We use the observed timing of these B peak encounters to estimate an average magnetopause speed along the magnetopause normal direction relative to TH-B. The times of peak B observations, corresponding probe locations, time differences and probe separations relative to TH-B are shown in Table 2 together with the derived average normal speed of the assumed magnetopause. The normal speeds ranged from 45.6 to 67.9 km/s. The maximum speed was that between TH-B and its closest neighbor (TH-D) while the lowest speed was found between TH-B and TH-A. This indicates that the magnetopause speed was slowing down as it expanded outward from TH-B toward TH-A.

3. THEMIS-A Observations

[23] Clear evidence of magnetopause surface waves is provided by the TH-A observations during the 0640–0800 UT period shown in Figure 6. This was indicated by the numerous TH-A crossings between the PDL (high B, low Ti) immediately outside the magnetopause and the LLBL (low B, high Ti). At least 28 short-duration LLBL events occurred during the 67-min-long 0653–0800 UT period in Figure 6. This corresponds to 56 magnetopause transitions or on average 1.2 minutes between transitions. The subsequent 0800–0850 UT period was characterized by ~62 LLBL-PDL transitions (not shown) in 50 min or 48 s on average between magnetopause encounters.

[24] The measured magnetic field and velocity in GSM coordinates between 0640 and 0800 UT were transformed into a local boundary normal LMN coordinate system [*Russell and Elphic*, 1978] based on a *Fairfield* [1971] model magnetopause normal relative to the TH-A GSM position. The local $\hat{\mathbf{N}}_{GSM}$ points outward from the magnetopause and $\hat{\mathbf{M}}_{GSM}$ points sunward along the magnetopause in the $Z_{GSM} = 0$ plane and perpendicular to $\hat{\mathbf{N}}_{GSM}$. $\hat{\mathbf{L}}_{GSM}$ completes a right-handed system and points in a generally northward direction along Z_{GSM}. The local LMN system directions naturally change somewhat with the TH-A position.

[25] The normal velocity V_N displayed in Figure 6g clearly indicates a measured outward plasma motion during the 0648–0650 UT period with an average V_N = 52.9 km/s (maximum V_N = 61.0 km/s and minimum V_N = 42.8 km/s). The average 52.9 km/s normal speed is consistent with the estimated outward 45.6–67.9 km/s normal magnetopause speed from the compressed PDL field magnitude encountered by THEMIS (see Figure 5) at this same time. Each individual magnetopause transition shown in Figure 6 typically confirms the presence of surface waves on the basis of V_N. The PDL-to-LLBL transitions generally coincide with an increasing or positive V_N while a decreasing or negative V_N typically occurred for the opposite LLBL-to-PDL transitions.

[26] A key TH-A observation was the relatively common and narrow bipolar signatures in the normal magnetic field component (B_N, positive toward the magnetosheath) as TH-

Table 2. Velocity of Peak B Signals Along the TH-B Normal Direction on 8 June 2007[a]

THEMIS	Time (UT)	GSM Position[b] (R_E)	ΔT (s)	ΔR (R_E)	V_N^{MP} (km/s)
TH-B	0647:41	(6.65, 10.26, −3.19)	–[c]	–[c]	–[c]
TH-D	0648:25	(7.18, 10.36, −3.30)	44.0	0.5444	67.9
TH-C	0648:55	(7.36, 10.42, −3.36)	74.0	0.7414	56.0
TH-E	0649:15	(7.53, 10.49, −3.41)	94.0	0.9260	55.8
TH-A	0650:46	(8.21, 10.47, −3.48)	185.0	1.5933	45.6

[a]TH-B unit normal vector $\hat{\mathbf{N}}^B_{GSM}$ = (0.7241, 0.6586, −0.2049).
[b]One Earth radius is defined as R_E = 6378.16 km.
[c]ΔT, ΔR, and V_N^{MP} are all relative to TH-B.

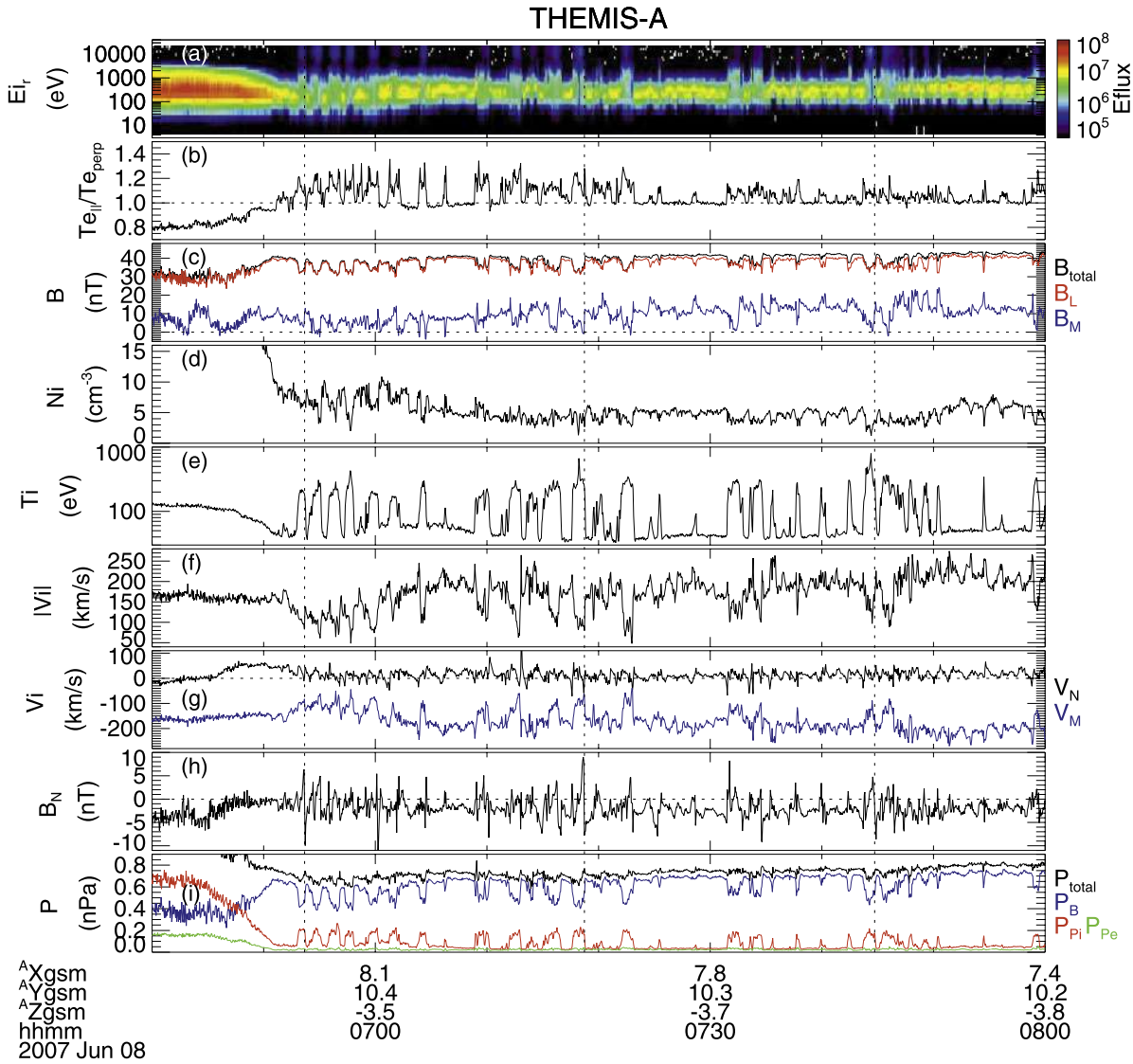

Figure 6. TH-A ESA and FGM instrument observations during the 0640–0800 UT period on 8 June 2007. (a) Ion energy-time spectrogram (energy flux in eV/cm^2 s sr eV), (b) electron temperature anisotropy ratio, (c) total magnetic field strength (black) and two components of the magnetic field in boundary normal coordinates B_L (red, positive along Z_{GSM}) and B_M (blue, positive sunward along the magnetopause), (d) ion density, (e) average ion temperature, (f) ion flow speed, (g) ion velocity along the nominal outward magnetopause normal (V_N, black) and along the sunward pointing V_M direction (blue), (h) normal B_N magnetic field component, and (i) plasma and magnetic field pressures as indicated ($P_{total} = P_B + P_{Pi} + P_{Pe}$).

A moved from the LLBL into the PDL. We have indicated the center of three such events in Figure 6 (dotted vertical lines at 0653:40, 0718:44 and 0744:44 UT). They were not related to any major plasma acceleration on either side of the local magnetopause and the Walén relation [e.g., *Sonnerup et al.*, 1987] was not satisfied for any of them.

[27] The bipolar B_N feature appeared to be less common at the other transitions from the PDL into the LLBL, where on the other hand TH-A was more likely to observe enhanced downtail plasma speeds ($V_M < 0$). This plasma acceleration may not necessarily be related to reconnection as suggested by the failure to find any event that satisfied the Walén relation. The acceleration could be a consequence of the introduction of KH waves into the subsonic magnetosheath flow such that the flow is forced around this obstacle. The flow should get decelerated and compressed at the trailing (sunward) edge of the wave, while it gets accelerated and decompressed at the leading (antisunward) side of the KH wave. This anticorrelation between V_M and N_P was not generally observed at the boundaries. Other mechanisms have been proposed for plasma acceleration along the magnetopause related to magnetic tension effects or magnetic pressure gradients during northward IMF [e.g., *Chen et al.*, 1993; *Lavraud et al.*, 2007] which could explain the tailward acceleration at these PDL-to-LLBL boundaries.

[28] The center of each small-scale bipolar B_N event was generally related to a local increase of the total plasma pressure P_{total} as illustrated in Figure 6i. We therefore suggest

Table 3. Average LLBL and PDL Magnetic Field for Three FTE Events

Event	Center Time (UT)	LLBL Time[a] (UT)	PDL Time[a] (UT)	$\mathbf{B}_{GSM}^{LLBL}$ (nT)	$\mathbf{B}_{GSM}^{PDL}$ (nT)	Shear Angle (deg)
FTE1	0653:40	0653:23	0653:56	(8.6, 1.0, 31.7)	(11.1, −3.6, 37.7)	7.0
FTE2	0718:44	0718:21	0719:03	(9.3, 0.6, 30.8)	(10.5, −6.0, 38.6)	9.8
FTE3	0744:44	0744:19	0745:01	(10.9, 1.6, 32.0)	(12.4, −4.2, 40.0)	8.6

[a]Times in LLBL and PDL are midpoints of 6-s average periods.

that the B_N features observed at the trailing (sunward) edges of these surface waves are small FTEs. They were in fact smaller than the 0640–0800 UT average 0.56 R_E normal distance between TH-A and TH-E, since no individual FTE could be clearly identified at TH-E within $\Delta t \sim$30 s of each TH-A event. Here, $\Delta t = \Delta R_M / V_M$, ΔR_M = 0.44 R_E is the average distance along the magnetopause from TH-A to TH-E and $V_M \sim$ 100 km/s is the minimum plasma speed at the time of the FTEs (see Figure 6).

[29] Time-dependent reconnection is often proposed for FTE generation [e.g., *Scholer*, 1988]. However, an antiparallel field component is required across the current sheet for this process to proceed. The locally obtained magnetic field shear angles at TH-A for the three FTEs indicated in Figure 6 were 7.0°, 9.8° and 8.6° across the respective magnetopause boundaries with By_{GSM} providing the antiparallel component (see Table 3). The low shear angles compare well with the mean 8.3° ± 5.2° shear angle distribution for 19 magnetopause crossings in the 0650–0735 UT time period.

4. THEMIS-A Reconstruction Analysis

[30] The structure of the magnetopause boundary layer surrounding the bipolar B_N signature observed by TH-A at 0653:40 UT is studied using two methods for a reconstruction of two-dimensional (2-D) maps of the magnetic and velocity fields from single-spacecraft measurements. The first technique recovers streamlines using a Grad-Shafranov-like (GS-like) equation for the compressible stream function as developed by *Sonnerup et al.* [2006] and first applied by *Hasegawa et al.* [2007a]. The second technique permits a reconstruction of both streamlines and magnetic field lines directly from the ideal 2-D MHD equations [*Sonnerup and Teh*, 2008]. It is referred to here as MHD reconstruction. Both techniques generate maps of streamlines (for MHD reconstruction, also magnetic field lines) and other plasma parameters in a rectangular domain surrounding the spacecraft x axis trajectory by using measured data as spatial initial values. The basic assumptions for both methods are that the structures encountered are 2-D and that they are time-independent when analyzed in their proper moving frame of reference. These assumptions are never precisely satisfied in any real applications, but experiments using synthetic data from time-dependent 2-D or 3-D numerical simulations indicate that the reconstructions nevertheless can produce qualitatively correct streamline and field line patterns [*Hasegawa et al.*, 2007a, 2007b].

[31] Figure 7 shows the GS-like map of streamlines in the reconstruction xy plane derived from data that TH-A obtained during the 93-s-long interval between 0653:16 and 0654:49 UT. The white arrows along the x axis correspond to the measured TH-A velocity transformed into the comoving frame of reference. The invariant (z) axis orientation and the velocity of the comoving frame (in which the reconstruction is performed) were determined using a method developed by *Sonnerup and Hasegawa* [2005]. The resulting frame velocity is $\mathbf{V}_0$ = (−55.1, 90.6, 14.8) km/s (GSE) which is roughly antiparallel (167°) to the average $\hat{\mathbf{M}}_{GSM}$ = (0.663, −0.749, 0.000) direction of the LMN boundary normal coordinate system at TH-A during this 93-s-long period. This indicates that the reconstructed features in Figure 7 were propagating tailward along the postnoon magnetopause. The x axis of the map is approximately antiparallel to $\mathbf{V}_0$ but it was rotated about the z axis by ∼3.2° relative to $\mathbf{V}_0$ to yield a well-organized map. The frame speed along the x axis is −107.1 km/s.

[32] The GS-like streamline map fully reveals a large plasma flow vortex (length ∼1 R_E and width ∼2000 km) along the x axis and centered at x ∼7500 km. It is inferred from the frequent boundary traversals (see Figure 6) that a second large vortex was present (centered at some negative x value), but only partially visible on this map. An elon-

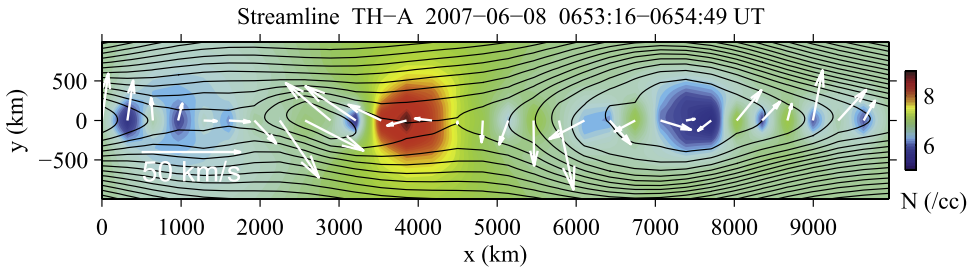

Figure 7. Map of streamlines (black lines) recovered from TH-A observations during a 93-s-long (0653:16–0654:49 UT) interval on 8 June 2007 with reconstructed density in color. White arrows show measured velocity vectors, transformed into the comoving frame (see text for details). The subsolar region is to the right, and the magnetosheath region is on top. GSE components of the reconstruction coordinates are x = (0.46842, −0.87478, −0.12387), y = (0.83442, 0.48411, −0.26342), and z = (0.29040, 0.02003, 0.95670).

gated and smaller vortex was centered at $x \sim 2700$ km between these two large vortices. It is embedded within the boundary layer and tilted relative to it. The bipolar magnetic perturbation observed by TH-A at 0653:40 UT was seen during the passage of this small vortex as discussed below. GS-like reconstructions of TH-A data for later intervals also demonstrate the presence of vortices with a similar size and aspect ratio (~ 1 R_E by 2000 km), suggesting that KH waves were propagating along the postnoon magnetopause throughout the 0650–0900 UT period. The encountered KH waves do not appear rolled up yet since the amplitude of the reconstructed waves (transverse y width of the vortices) is still rather small ($\sim$2000 km) as compared to the 1 R_E wavelength.

[33] Periodic magnetopause transitions between the LLBL and the PDL were seen mainly at the outermost TH-A probe during the 0650–0900 UT period and occasionally also at the inner TH-C, D and E probes. The probe separations during the second 5-min interval analyzed in Table 1 suggest a KH wave amplitude in the range $0.18 < D_{MP} < 0.91$ R_E or $1157 < D_{MP} < 5776$ km along the local magnetopause direction, since neither TH-A nor TH-D observed a continuous magnetopause wave activity. A wave amplitude in this range is consistent with the reconstructed $\sim$2000 km transverse width and strongly suggests that the KH waves were still in an early growth phase in agreement with statistical results showing that rolled up vortices are seen predominantly behind the dawn-dusk terminator [*Hasegawa et al.*, 2006a]. The magnetosheath ion population, when observed in the LLBL during this event, is therefore unlikely to be a result of local plasma entry produced by the nonlinear KHI [*Hasegawa et al.*, 2004]. Direct penetration of the dayside magnetosheath plasma due to high-latitude reconnection tailward of both cusps [e.g., *Song and Russell*, 1992; *Øieroset et al.*, 2008; *McFadden et al.*, 2008b] is a more likely explanation, given the prevailing northward IMF conditions.

[34] Figure 8 shows maps of streamlines (first and second panels) and magnetic field lines (third panel) recovered from an MHD reconstruction of the shorter 0653:16–0654:04 UT time interval during which the 0653:40 UT bipolar B_N feature occurred. White arrows along $y = 0$ are the observed TH-A velocity vectors (first and second panels) and the magnetic field vectors (third panel) projected onto the reconstruction plane. The reconstruction axes and the comoving $\mathbf{V}_0$ frame velocity are the same as those used for the GS-like reconstruction. The MHD reconstruction results indicate that the recovered streamline map is qualitatively similar to the $x = 0$–5000 km range of the GS-like reconstruction results in Figure 7. However, the small vortex centered at $x = 2700$ km is less elongated than its counterpart in Figure 7. The fact that the small vortex occurs in both reconstructions, despite the very different techniques, indicates that it is a robust feature.

[35] Unlike the GS-like approach, xy plane magnetic field components are self-consistently calculated in the MHD reconstruction. The third panel of Figure 8 displays the recovered magnetic field map (axial B_z magnetic field in color), which shows a coherent magnetic island structure embedded within the LLBL just inside the magnetopause boundary. High B_z values indicate the adjacent PDL region in agreement with observations (see Figure 6). The island is consistent with the bipolar B_N signature (white arrows) that TH-A observed. A magnetic island was also recovered (not shown) for the same interval by use of the magnetohydrostatic GS reconstruction technique [*Hau and Sonnerup*, 1999]. The island thus appears to be a robust feature of the reconstruction.

[36] The fourth panel in Figure 8 shows a combined map of streamlines and field lines. It indicates that although the two sets are qualitatively similar, there is a relative displacement between the magnetic island and the small plasma vortex. The magnetic island appears near a topological X point in the transverse magnetic field (located at $x \sim 1200$ km) and a nearly coincident hyperbolic X point of the streamline pattern. However, the flow behavior near the magnetic X point does not contain the bidirectional jetting, nor the general flow pattern, expected at an active reconnection site. Since streamlines and field lines would coincide in a steady state 2-D configuration in the absence of reconnection, these facts indicate that there is some modest temporal evolution of the field structure. The magnetic field lines are stretched and moved around by the plasma flow. The flow, in turn, is also modified by the stresses associated with the in-plane magnetic field. The reconstruction maps should therefore be thought of as time-aliased for this event. However, we believe that they are qualitatively correct snapshots of the field and flow configuration. As a result of the stretching by the vortex flow, the magnetic island is elongated at an angle to the x axis.

[37] Although the maps of density, temperature, and axial magnetic field (the first, second, and third panels in Figure 8) are somewhat corrupted by the absence of a static equilibrium, they nevertheless show qualitative behavior that is realistic. In the middle of the map, there is a transition from a region of low density, high temperature and low axial field (LLBL) to a region of high density, low temperature and high axial field (PDL) consistent with TH-A observations (see Figure 6). Throughout most of the map, the axial field is approximately conserved along field lines as expected in the magnetohydrostatic limit when the dynamic effects of the flow are small.

[38] To further check the validity of the MHD reconstruction results, it is useful to examine the behavior of the measured convection electric field, after it has been transformed to the moving reconstruction frame. Figure 9 shows the components of this field along its maximum, intermediate, and minimum variance directions. The last of these directions is along the chosen invariant z axis while the other two lie in the reconstruction (xy) plane. In a steady 2-D field configuration, Faraday's law requires the axial electric field to be strictly constant. Figure 9 shows that this is nearly the case so that the base assumptions of the reconstruction results are well satisfied and the proper frame axis orientation and motion has been found. The axial electric field component is very small (-0.012 mV/m on average) but contains small fluctuations with a standard deviation of 0.023 mV/m. These fluctuations are associated with the temporal evolution discussed above. The average axial electric field component could in principle be caused by reconnection at the magnetic X point. It has the expected negative sign, but its magnitude is too small to be considered significant. Although it is reasonable to assume that the

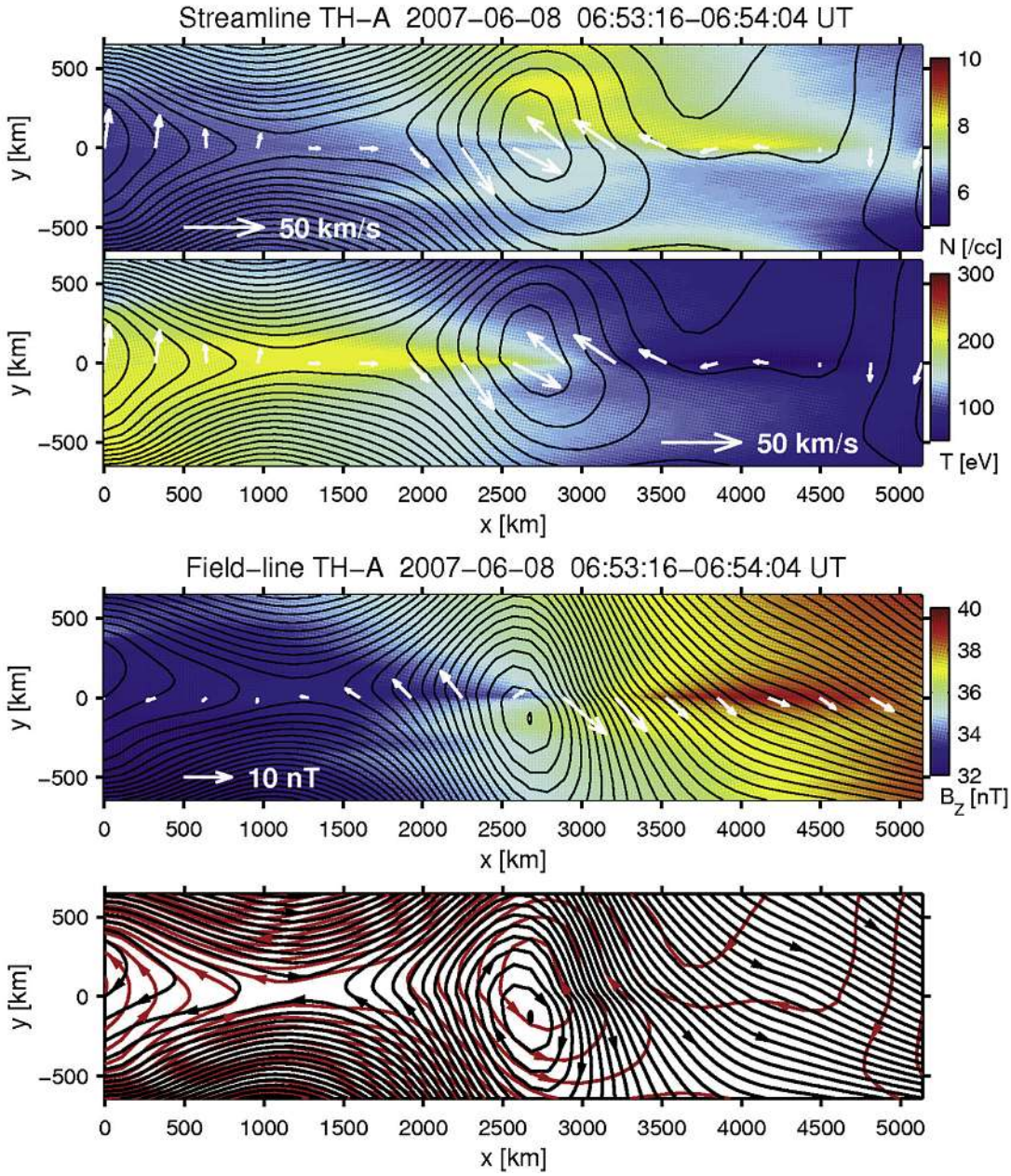

Figure 8. Maps of streamlines (black, first and second panels) and field lines (black, third panel) from the MHD reconstruction using a shorter (0653:16–0654:04 UT) interval of TH-A data. The fourth panel shows an overlay of streamlines (red) and field lines (black). In the first and second panels, the ion density and temperature are shown in color, and white arrows are measured velocity vectors, transformed into the comoving frame and projected onto the reconstruction *xy* plane. In the third panel, the axial field (B_z) is in color, and white arrows are measured field vectors, projected onto the *xy* plane. The magnetosheath PDL is toward the top, and the magnetosphere is toward the bottom of the reconstruction domain. The subsolar region is toward the bottom right.

magnetic island was created by a burst of reconnection at this *X* point, the reconnection activity must have occurred at an earlier time, i.e., at some upstream location on the magnetopause. At the time the *X* point and the island reached TH-A, the reconnection activity had essentially ceased. This type of situation also arises for standard FTE flux ropes, observed at high latitudes, well away from the time and place where they were created [*Hasegawa et al.*, 2006b].

[39] One question that arises concerning the growth of the KH waves is whether the spatial growth rate, which cannot be captured in reconstructions based on data from a single spacecraft, could be large enough to seriously compromise the various features we have discussed in the reconstruction maps. Although we cannot completely exclude this possibility, we note that the reconstruction by *Hasegawa et al.* [2007a] of a numerically simulated 2-D KH vortex indicates that meaningful streamlines can be recovered even in the

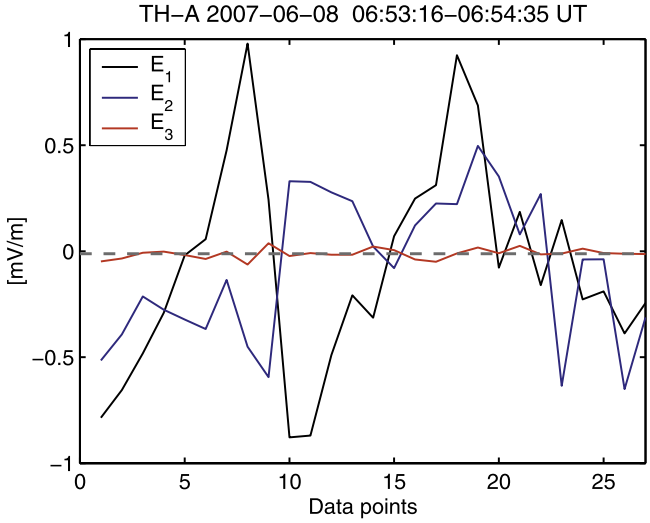

Figure 9. Derived convection electric field components in variance coordinates. E_1, E_2, and E_3 are the electric field values along the maximum, intermediate, and minimum variance directions, respectively. The variance coordinates are obtained using the method described by *Sonnerup and Hasegawa* [2005]. The minimum variance direction is the same as the invariant axis used in the MHD reconstruction. The axial electric field (E_3) is denoted by a red line, and its average ($\sim -0.012 \pm 0.023$ mV/m) is shown by a dashed line.

presence of substantial time evolution. Linear growth times for the KHI, predicted from 2-D theory or simulations in the absence of a PDL, are comparable to, or shorter than, the time intervals used in the reconstructions we have presented. However, it is unclear how applicable such predictions are to a real magnetopause region with an adjacent PDL, where 3-D effects such as field line bending and stretching caused by flow shear across, and acceleration along, the magnetopause may act to stabilize the KH growth.

5. Summary and Conclusions

[40] THEMIS observations at the postnoon magnetopause show for the first time that small-scale < 0.56 R_E FTEs were common at the trailing (sunward) edges of KH waves in their growth phase during a ~2-h-long period of TH-A observations between 0650 and 0910 UT on 8 June 2007 when the IMF was predominantly northward. In situ FTE evidence consists of enhanced total plasma pressure at the center of the bipolar B_N features as TH-A moved from the LLBL into a local magnetosheath PDL adjacent to the magnetopause. Bipolar B_N features were only occasionally observed at the opposite (leading edge of the surface waves) magnetopause transition from the PDL into the LLBL.

[41] MHD as well as Grad-Shafranov based reconstructions confirmed the presence of a magnetic island which was associated with a small plasma flow vortex within the LLBL just inside the local magnetopause for two FTE events observed by TH-A at 0653:40 and 0718:44 UT (not shown). The Grad-Shafranov-like streamline reconstruction map provides a large-scale context for the MHD reconstruction maps of density, temperature, axial magnetic field and in-plane magnetic field contours that confirm the appearance of a magnetic island between two larger-scale KH vortices. These vortices were not yet rolled up on the basis of these THEMIS observations.

[42] Because of the large kinetic energy of the magnetosheath flow along the magnetospheric flanks, it is clear that the KHI can develop even in the presence of the small magnetic field components present in the reconstruction plane. The resulting vortices deform this field so as to create local regions in which there are spatially rapid reversals of the in-plane field. At such sites reconnection of the in-plane field can then take place, leading to the formation of magnetic islands, or more precisely, magnetic flux ropes. The guide field (the z component) in these ropes is much stronger than the circumferential field, but there is no reason to assume that the guide field would prevent reconnection from occurring. Low-shear reconnection is indeed frequently observed in interplanetary space [*Gosling et al.*, 2007] and also occurs in tokamak devices.

[43] More specifically, with support from the TH-A MHD reconstruction results in Figure 8 and the low $\beta_i < 0.2$ observed within the PDL (see Figure 3), we propose that the small-scale FTEs may have been generated in the early growth phase of the KHI in the vicinity of the postnoon TH-A location due to pulse-like low-shear reconnection [*Paschmann et al.*, 1986] between magnetosheath (PDL) and magnetospheric fields at the trailing (sunward) edges of the growing KH surface waves. This is a topologically different merging scenario than that proposed, e.g., by *Nykyri and Otto* [2004], in which reconnection occurs between fields of magnetosheath (or magnetospheric) origin during the nonlinear phase of rolled up KH vortices, typically behind the terminator. The observed sunward edge preference of the small FTEs is consistent with a localized compression of the magnetopause current sheet due to converging vortex flow at the hyperbolic point between neighboring larger-scale KH vortices (see Figures 7 and 8) as a triggering mechanism for the proposed reconnection process. A similar scenario was proposed by *Nakamura et al.* [2006, 2008] on the basis of numerical simulations, although at a later stage of the KHI. The small plasma vortex that we found to be associated with the reconstructed FTE most likely developed as a byproduct of the reconnection process and of the stresses associated with the in-plane magnetic field of the deforming magnetic island.

[44] **Acknowledgments.** We thank R. P. Lepping, R. P. Lin, and K. W. Ogilvie for the use of Wind data and D. J. McComas for use of the ACE SWEPAM plasma data made available via the CDAWeb. We thank the ACE MAG instrument team and the ACE Science Center for providing the ACE Level 2 data via http://www.srl.caltech.edu/ACE/ASC/level2/. Work by S.E. was supported by a THEMIS subaward to LASP (NASA grant NAS5-02099) at the University of Colorado at Boulder. Work by W.-L.T. and B.U.Ö.S. was supported by NASA Cluster Theory Guest Investigator grant NNG-05GG26G to Dartmouth College.

[45] Wolfgang Baumjohann thanks the reviewers for their assistance in evaluating this paper.

References

Anderson, B. J., and S. A. Fuselier (1993), Magnetic pulsations from 0.1 to 4.0 Hz and associated plasma properties in the Earth's subsolar magnetosheath and plasma depletion layer, *J. Geophys. Res.*, *98*, 1461.

Anderson, B. J., T.-D. Phan, and S. A. Fuselier (1997), Relationships between plasma depletion and subsolar reconnection, *J. Geophys. Res.*, *102*, 9531.

Angelopoulos, V. (2008), The THEMIS mission, *Space Sci. Rev.*, *141*, 5, doi:10.1007/s11214-008-9336-1.

Auster, H. U., et al. (2008), The THEMIS Fluxgate Magnetometer, *Space Sci. Rev.*, *141*, 235, doi:10.1007/s11214-008-9365-9.

Brackbill, J. U., and D. A. Knoll (2001), Transient magnetic reconnection and unstable shear layers, *Phys. Rev. Lett.*, *86*, 2329, doi:10.1103/PhysRevLett.86.2329.

Chen, S.-H., M. G. Kivelson, J. T. Gosling, R. J. Walker, and A. J. Lazarus (1993), Anomalous aspects of magnetosheath flow and of the shape and oscillations of the magnetopause during an interval of strongly northward interplanetary magnetic field, *J. Geophys. Res.*, *98*, 5727.

Cully, C. M., R. E. Ergun, K. Stevens, A. Nammari, and J. Westfall (2008), The THEMIS Digital Fields Board, *Space Sci. Rev.*, *141*, 343, doi:10.1007/s11214-008-9417-1.

Dungey, J. W. (1963), The structure of the exosphere, or adventures in velocity space, in *Geophysics: The Earth's Environment*, edited by C. DeWitt, J. Hieblot, and A. Lebeau, p. 503, Gordon and Breach, New York.

Fairfield, D. H. (1971), Average and unusual locations of the Earth's magnetopause and bow shock, *J. Geophys. Res.*, *76*, 6700.

Fairfield, D. H., A. Otto, T. Mukai, S. Kokubun, R. P. Lepping, J. T. Steinberg, A. J. Lazarus, and T. Yamamoto (2000), Geotail observations of the Kelvin-Helmholtz instability at the equatorial magnetotail boundary for parallel northward fields, *J. Geophys. Res.*, *105*, 21,159.

Fujimoto, M., and T. Terasawa (1994), Anomalous ion mixing within an MHD scale Kelvin-Helmholtz vortex, *J. Geophys. Res.*, *99*, 8601.

Gosling, J. T., T. D. Phan, R. P. Lin, and A. Szabo (2007), Prevalence of magnetic reconnection at small field shear angles in the solar wind, *Geophys. Res. Lett.*, *34*, L15110, doi:10.1029/2007GL030706.

Hasegawa, H., M. Fujimoto, T.-D. Phan, H. Rème, A. Balogh, M. W. Dunlop, C. Hashimoto, and R. TanDokoro (2004), Transport of solar wind into Earth's magnetosphere through rolled-up Kelvin-Helmholtz vortices, *Nature*, *430*, 755.

Hasegawa, H., M. Fujimoto, K. Takagi, Y. Saito, T. Mukai, and H. Rème (2006a), Single-spacecraft detection of rolled-up Kelvin-Helmholtz vortices at the flank magnetopause, *J. Geophys. Res.*, *111*, A09203, doi:10.1029/2006JA011728.

Hasegawa, H., B. U. Ö. Sonnerup, C. J. Owen, B. Klecker, G. Paschmann, A. Balogh, and H. Rème (2006b), The structure of flux transfer events recovered from Cluster data, *Ann. Geophys.*, *24*, 603.

Hasegawa, H., B. U. Ö. Sonnerup, M. Fujimoto, Y. Saito, and T. Mukai (2007a), Recovery of streamlines in the flank low-latitude boundary layer, *J. Geophys. Res.*, *112*, A04213, doi:10.1029/2006JA012101.

Hasegawa, H., R. Nakamura, M. Fujimoto, V. A. Sergeev, E. A. Lucek, H. Rème, and Y. Khotyaintsev (2007b), Reconstruction of a bipolar magnetic signature in an earthward jet in the tail: Flux rope or 3D guide-field reconnection?, *J. Geophys. Res.*, *112*, A11206, doi:10.1029/2007JA012492.

Hau, L.-N., and B. U. Ö. Sonnerup (1999), Two-dimensional coherent structures in the magnetopause: Recovery of static equilibria from single-spacecraft data, *J. Geophys. Res.*, *104*, 6899.

Knoll, D. A., and J. U. Brackbill (2002), The Kelvin-Helmholtz instability, differential rotation, and three-dimensional, localized, magnetic reconnection, *Phys. Plasmas*, *9*, 3775, doi:10.1063/1.1494070.

Lavraud, B., M. F. Thomsen, M. G. G. T. Taylor, Y. L. Wang, T. D. Phan, S. J. Schwartz, R. C. Elphic, A. Fazakerley, H. Rème, and A. Balogh (2005), Characteristics of the magnetosheath electron boundary layer under northward interplanetary magnetic field: Implications for high-latitude reconnection, *J. Geophys. Res.*, *110*, A06209, doi:10.1029/2004JA010808.

Lavraud, B., J. E. Borovsky, A. J. Ridley, E. W. Pogue, M. F. Thomsen, H. Rème, A. N. Fazakerley, and E. A. Lucek (2007), Strong bulk plasma acceleration in Earth's magnetosheath: A magnetic slingshot effect?, *Geophys. Res. Lett.*, *34*, L14102, doi:10.1029/2007GL030024.

McFadden, J. P., C. W. Carlson, D. Larson, M. Ludlam, R. Abiad, B. Elliott, P. Turin, M. Marckwordt, and V. Angelopoulos (2008a), The THEMIS ESA plasma instrument and in-flight calibration, *Space Sci. Rev.*, *141*, 277, doi:10.1007/s11214-008-9440-2.

McFadden, J. P, T. D. Phan, C. W. Carlson, V. Angelopoulos, K.-H. Glassmeier, and U. Auster (2008b), Structure of the subsolar magnetopause regions during northward IMF: First results from THEMIS, *Geophys. Res. Lett.*, *35*, L17S09, doi:10.1029/2008GL033630.

Miura, A. (1984), Anomalous transport by magnetohydrodynamic Kelvin-Helmholtz instabilities in the solar wind-magnetosphere interaction, *J. Geophys. Res.*, *89*, 801.

Nakamura, T. K. M., M. Fujimoto, and A. Otto (2006), Magnetic reconnection induced by weak Kelvin-Helmholtz instability and the formation of the low-latitude boundary layer, *Geophys. Res. Lett.*, *33*, L14106, doi:10.1029/2006GL026318.

Nakamura, T. K. M., M. Fujimoto, and A. Otto (2008), Structure of an MHD-scale Kelvin-Helmholtz vortex: Two-dimensional two-fluid simulations including finite electron inertial effects, *J. Geophys. Res.*, *113*, A09204, doi:10.1029/2007JA012803.

Nykyri, K., and A. Otto (2001), Plasma transport at the magnetospheric boundary due to reconnection in Kelvin-Helmholtz vortices, *Geophys. Res. Lett.*, *28*, 3565.

Nykyri, K., and A. Otto (2004), Influence of the Hall term on KH instability and reconnection inside KH vortices, *Ann. Geophys.*, *22*, 935.

Nykyri, K., A. Otto, B. Lavraud, C. Mouikis, L. M. Kistler, A. Balogh, and H. Rème (2006), Cluster observations of reconnection due to the Kelvin-Helmholtz instability at the dawnside magnetospheric flank, *Ann. Geophys.*, *24*, 2619.

Øieroset, M., T. D. Phan, V. Angelopoulos, J. P. Eastwood, J. McFadden, D. Larson, C. W. Carlson, K.-H. Glassmeier, M. Fujimoto, and J. Raeder (2008), THEMIS multi-spacecraft observations of magnetosheath plasma penetration deep into the dayside low-latitude magnetosphere for northward and strong B_y IMF, *Geophys. Res. Lett.*, *35*, L17S11, doi:10.1029/2008GL033661.

Otto, A., and D. H. Fairfield (2000), Kelvin-Helmholtz instability at the magnetotail boundary: MHD simulation and comparison with Geotail observations, *J. Geophys. Res.*, *105*, 21,175.

Paschmann, G., G. Haerendel, I. Papamastorakis, N. Sckopke, S. J. Bame, J. T. Gosling, and C. T. Russell (1982), Plasma and magnetic field characteristics of magnetic flux transfer events, *J. Geophys. Res.*, *87*, 2159.

Paschmann, G., I. Papamastorakis, W. Baumjohann, N. Sckopke, C. W. Carlson, B. U. Ö. Sonnerup, and H. Lühr (1986), The magnetopause for large magnetic shear: AMPTE/IRM observations, *J. Geophys. Res.*, *91*, 11,099.

Paschmann, G., W. Baumjohann, N. Sckopke, T.-D. Phan, and H. Lühr (1993), Structure of the dayside magnetopause for low magnetic shear, *J. Geophys. Res.*, *98*, 13,409.

Phan, T. D., et al. (1996), The subsolar magnetosheath and magnetopause for high solar wind ram pressure: Wind observations, *Geophys. Res. Lett.*, *23*, 1279.

Phan, T. D., C. P. Escoubet, L. Rezeau, R. A. Treumann, A. Vaivads, G. Paschmann, S. A. Fuselier, D. Attié, B. Rogers, and B. U. Ö. Sonnerup (2005), Magnetopause processes, *Space Sci. Rev.*, *118*, 367, doi:10.1007/s11214-005-3836-z.

Pu, Z. Y., M. Yei, and Z. X. Liu (1990), Generation of vortex-induced tearing mode instability at the magnetopause, *J. Geophys. Res.*, *95*, 10,559.

Roux, A., O. Le Contel, C. Coillot, A. Bouabdellah, B. de la Porte, D. Alison, S. Ruocco, and M. C. Vassal (2008), The Search Coil Magnetometer for THEMIS, *Space Sci. Rev.*, *141*, 265, doi:10.1007/s11214-008-9455-8.

Russell, C. T, and R. C. Elphic (1978), Initial ISEE magnetometer results: Magnetopause observations, *Space Sci. Rev.*, *22*, 681.

Russell, C. T., and R. C. Elphic (1979), ISEE observations of flux transfer events at the dayside magnetopause, *Geophys. Res. Lett.*, *6*, 33.

Scholer, M. (1988), Strong core magnetic fields in magnetopause flux transfer events, *Geophys. Res. Lett.*, *15*, 748.

Sckopke, N., G. Paschmann, G. Haerendel, B. U. Ö. Sonnerup, S. J. Bame, T. G. Forbes, E. W. Hones Jr., and C. T. Russell (1981), Structure of the low-latitude boundary layer, *J. Geophys. Res.*, *86*, 2099.

Sibeck, D. G., R. P. Lepping, and A. J. Lazarus (1990), Magnetic field line draping in the plasma depletion layer, *J. Geophys. Res.*, *95*, 2433.

Song, P., and C. T. Russell (1992), Model of the formation of the low-latitude boundary layer for strongly northward interplanetary magnetic field, *J. Geophys. Res.*, *97*(A2), 1411.

Sonnerup, B. U. Ö. (1987), On the stress balance in flux transfer events, *J. Geophys. Res.*, *92*, 8613.

Sonnerup, B. U. Ö., and H. Hasegawa (2005), Orientation and motion of two-dimensional structures in a space plasma, *J. Geophys. Res.*, *110*, A06208, doi:10.1029/2004JA010853.

Sonnerup, B. U. Ö., and W.-L. Teh (2008), Reconstruction of two-dimensional MHD structures in a space plasma: The theory, *J. Geophys. Res.*, *113*, A05202, doi:10.1029/2007JA012718.

Sonnerup, B. U. Ö., I. Papamastorakis, G. Paschmann, and H. Lühr (1987), Magnetopause properties from AMPTE/IRM observations of the convection electric field: Method development, *J. Geophys. Res.*, *92*, 12,137.

Sonnerup, B. U. Ö., H. Hasegawa, W.-L. Teh, and L.-N. Hau (2006), Grad-Shafranov reconstruction: An overview, *J. Geophys. Res.*, *111*, A09204, doi:10.1029/2006JA011717.

Tsurutani, B. T., E. J. Smith, R. R. Anderson, K. W. Ogilvie, J. D. Scudder, D. N. Baker, and S. J. Bame (1982), Lion roars and nonoscillatory drift mirror waves in the magnetosheath, *J. Geophys. Res.*, *87*, 6060.

Wang, Y. L., J. Raeder, C. T. Russell, T. D. Phan, and M. Manapat (2003), Plasma depletion layer: Event studies with a global model, *J. Geophys. Res.*, *108*(A1), 1010, doi:10.1029/2002JA009281.

Zwan, B. J., and R. A. Wolf (1976), Depletion of solar wind plasma near a planetary boundary, *J. Geophys. Res.*, *81*, 1636.

V. Angelopoulos, C. W. Carlson, D. E. Larson, and J. P. McFadden, Space Sciences Laboratory, University of California, 7 Gauss Way, Berkeley, CA 94720-7450, USA. (vassilis@ssl.berkeley.edu; cwc@ssl.berkeley.edu; davin@ssl.berkeley.edu; mcfadden@ssl.berkeley.edu)

C. M. Cully, Swedish Institute of Space Physics, Box 537, SE-75121 Uppsala, Sweden. (chris@irfu.se)

R. E. Ergun and S. Eriksson, Laboratory for Atmospheric and Space Physics, University of Colorado, 1234 Innovation Drive, Boulder, CO 80303-7814, USA. (ree@lasp.colorado.edu; eriksson@lasp.colorado.edu)

K.-H. Glassmeier, Institut für Geophysik und Extraterrestrische Physik, Technische Universität, Mendelssohnstrasse 3, D-38106 Braunschweig, Germany. (kh.glassmeier@tu-braunschweig.de)

H. Hasegawa, Department of Space Plasma Physics, Institute of Space and Astronautical Science, Japan Aerospace Exploration Agency, 3-1-1 Yoshinodai, Sagamihara 229-8510, Japan. (hase@stp.isas.jaxa.jp)

O. Le Contel and A. Roux, Laboratoire de Physique des Plasmas, École Polytechnique, Route de Saclay, F-91128 Palaiseau, France. (olivier.lecontel@cetp.ipsl.fr; alain.roux@cetp.ipsl.fr)

B. U. Ö. Sonnerup and W.-L. Teh, Thayer School of Engineering, Dartmouth College, 8000 Cummings Hall, Hanover, NH 03755-8000, USA. (bengt.u.o.sonnerup@dartmouth.edu; wai-leong_teh@dartmouth.edu)